Subangstrom Free-Electron Laser Operation with Undulator Deflection Parameter Reaching the Subunity Regime

Eduard Prat,[1,*] Christopher Arrell,[2] Marco Calvi,[2] Nicole Hiller,[1] Pavle Juranić,[1] Christoph Kittel,[1] Sven Reiche,[1] Thomas Schietinger,[1] Didier Voulot,[1] and Tobias Weilbach[1]

[1]PSI Center for Accelerator Science and Engineering, Paul Scherrer Institute, 5232 Villigen PSI, Switzerland
[2]PSI Center for Photon Science, Paul Scherrer Institute, 5232 Villigen PSI, Switzerland

(Received 17 March 2026; accepted 17 August 2026; published 11 September 2026; corrected 23 October 2026)

X-ray free-electron lasers (XFELs) enable the exploration of matter with atomic-scale spatiotemporal resolution. Generating radiation wavelengths below one angstrom is critical for applications such as crystallography and Mössbauer studies. Until now, achieving the subangstrom regime has required electron beam energies ≥ 8 GeV and undulator K parameters ≥ 1.5. In this Letter, we demonstrate the generation of high-power subangstrom FEL radiation using a 6.2 GeV electron beam and a K parameter around unity and below. We show that exceptional electron beam brilliance—characterized by high peak current and low slice emittance—compensates for the reduced undulator coupling, enabling robust lasing. The demonstration was carried out at SwissFEL, where the subangstrom regime has already been successfully employed in user experiments. Our Letter paves the way for more compact and cost-effective accelerator designs through the optimization of electron beam quality.

DOI: 10.1103/dv32-v967

X-ray free-electron lasers (XFELs) enable cutting-edge research across structural biology, femtochemistry, and condensed matter physics [1,2] by producing intense femtosecond pulses at angstrom and subangstrom wavelengths. This radiation is generated as a high-brilliance (or brightness) electron beam traverses an undulator, where the fundamental wavelength λ is determined by the resonance condition $\lambda = (\lambda_u/2\gamma^2)[1 + (K^2/2)]$ [3]. Here, λ_u is the undulator period, K is the dimensionless deflection parameter, and $\gamma = E/(m_e c^2)$ is the electron Lorentz factor, with E being the beam energy and $m_e c^2 = 0.511$ MeV.

Efficient FEL amplification requires strict electron beam quality and alignment. Transversely, the normalized emittance ε_n must satisfy $(\varepsilon_n/\gamma) \leq [\lambda/(4\pi)]$ [4], while longitudinally, the uncorrelated relative energy spread σ_γ/γ must be smaller than the Pierce parameter [3] (10^{-4} to 10^{-3} in the hard x-ray regime). Furthermore, achieving high power and short saturation lengths demands a high effective Pierce parameter [5], which is maximized by high beam brilliance (high peak current, low emittance, low energy spread) combined with longer undulator periods and higher K values. Consequently, standard XFELs operate with K values well above unity, as lower K values reduce the electron-photon coupling. While higher beam energies, longer periods, and larger K values optimize FEL performance, they inherently necessitate larger facilities with significantly higher construction and operational costs.

There are currently five XFEL facilities worldwide that operate in the hard x-ray regime: LCLS (USA) [6] with its high-repetition rate upgrade LCLS-II [7], SACLA (Japan) [8], PAL-XFEL (South Korea) [9], the European XFEL (Germany) [10], and SwissFEL, operating at the Paul Scherrer Institute in Switzerland [11]. Furthermore, SHINE (China) [12] is currently under construction and commissioning. The electron beam energies range from around 6 GeV at SwissFEL to 17.5 GeV at the European XFEL. To achieve a given radiation wavelength, facilities with lower electron beam energies must operate with shorter undulator periods. For instance, the hard-x-ray beamline at SwissFEL utilizes undulators with a 15 mm period, whereas the European XFEL employs a 40 mm period. Furthermore, the requirements for normalized transverse emittance and absolute energy spread become increasingly stringent for facilities operating at lower electron beam energies.

LCLS, SACLA, the European XFEL, and PAL-XFEL all currently provide subangstrom radiation to their scientific users. A notable example is SACLA, which reported the production of FEL radiation at 0.73 Å (17 keV photon energy) with pulse energies at the 10 μJ level, increasing to approximately 50 μJ at 0.89 Å (14 keV) [8]. More recent studies have reported pulse energies of 160 μJ at 0.83 Å [13]. This was achieved with an electron beam energy of 8.3 GeV, an undulator beamline comprising 18 modules

*Contact author: eduard.prat@psi.ch

Published by the American Physical Society under the terms of the Creative Commons Attribution 4.0 International license. Further distribution of this work must maintain attribution to the author(s) and the published article's title, journal citation, and DOI.

(5 m each) with a period of 18 mm, and K values of 1.5 or higher. In contrast, LCLS, the European XFEL, and PAL-XFEL operate with higher electron beam energies, more extensive undulator beamlines, longer periods, and correspondingly higher K values.

The subangstrom regime enables enhanced spatial resolution, which is critical for applications such as high-resolution crystallography [13] and time-resolved solution scattering [14]. Furthermore, extending the wavelength range below one angstrom provides access to higher-energy atomic core levels and specific excitation energies required for nuclear resonance techniques. A prominent example is the Mössbauer transition of the ^{57}Fe isotope at 14.4 keV (0.86 Å) [15,16]. Moreover, these high photon energies are essential for pair distribution function analysis to study local atomic structure over a wide range of materials [17,18] and for penetrating complex sample environments such as diamond anvil cells [19].

SwissFEL was originally designed with a maximum electron beam energy of 5.8 GeV and an undulator period of 15 mm to produce radiation with wavelengths down to 1 Å (12.4 keV) at a K parameter of 1.2. During the early stages of operation, SwissFEL generated 1 Å radiation with 0.5 mJ pulse energies using a 6.2 GeV electron beam [11] and a K parameter of approximately 1.4. Following continuous facility-wide optimizations, we have recently achieved pulse energies exceeding 1 mJ at 1 Å wavelength [20]. In this Letter, we report the generation of high-intensity FEL radiation well into the subangstrom regime at SwissFEL. Specifically, we provide evidence for FEL radiation at a wavelength of 0.75 Å (16.5 keV) with pulse energies exceeding 100 μJ achieved by operating the existing undulator at a K value below 1 with an electron beam energy of 6.2 GeV. Furthermore, we reached pulse energies of approximately 400 μJ at a wavelength of 0.83 Å (15 keV) with a K value slightly above 1. This achievement is primarily attributed to the high brilliance of the electron beam, in particular its high peak current and small transverse emittance, which enables the generation of intense FEL radiation despite the reduced undulator coupling inherent to the low-K regime.

This regime has already been successfully utilized in small-molecule crystallography experiments at SwissFEL for a radiation wavelength of 0.84 Å (14.7 keV), both in standard and large-bandwidth [21] configuration, delivering typical pulse energies of 350 μJ (150 μJ with large bandwidth) over a 24-hour user shift, and it is expected to enter regular operation in the near future. Expanding the wavelength reach of the facility significantly enhances its scientific capacity and broadens the scope for high-energy x-ray research.

In a broader sense, the demonstration of robust lasing in the low K range proves that high-performance FEL operation is achievable even with weak undulator coupling. These results establish that electron beam brilliance can effectively compensate for reduced coupling strength, providing a clear roadmap for more compact and cost-effective future facilities. By prioritizing the quality of the electron beam over its energy, future XFEL facilities could access the x-ray regime with significantly lower electron beam energies. At the same time, existing facilities can leverage this approach to extend their spectral coverage without the need for costly linac upgrades. While the radiation power decreases at lower K values due to the nearly linear dependence of the power on the Pierce parameter, a qualitative scaling argument suggests that the photon brilliance remains approximately constant, since the FEL bandwidth also scales almost linearly with the Pierce parameter [1] assuming other beam parameters, such as photon source size and divergence, to remain unchanged.

The experiments were performed at Aramis, the hard x-ray beamline of SwissFEL [11], which is shown schematically in Fig. 1. The electron beam is generated in an rf photoinjector, compressed using magnetic chicanes (BC1 and BC2), and accelerated up to 6.2 GeV in the linac sections. The undulator line consists of 13 modules, each featuring a period length of 15 mm, a total length of 4 m, and a maximum K value of 1.8. The average β function in the undulator is 10 m. The electron beam properties are measured after linac 3 using a C-band transverse-deflecting structure (TDS) [22] and transverse profile monitors based on YAG scintillators [23,24]. Under typical operation conditions, the FEL radiation spectrum is monitored with a single-shot photon spectrometer [25]. However, this device is limited to photon energies below 13 keV (approximately 0.95 Å) and was, therefore, not applicable for the subangstrom radiation studies presented here. Instead, the average radiation spectrum was obtained from monochromator scans, with the output intensity recorded by a photodiode. The monochromator, which is located in the Bernina experimental beamline 100 m downstream of the undulator end, consists of a double silicon crystal system [Si(111)] [26,27]. The monochromator bandwidth is estimated to be 2 eV, and its wavelength calibration is verified via the crystal Bragg angle. The effects due to variations in Si(111) reflectivity and beamline transmission are negligible for our measurements. The average FEL pulse energy is measured directly with a photon gas monitor [28,29]



FIG. 1. Schematic of the SwissFEL hard x-ray line (not to scale).

placed 50 m downstream of the undulator end. Complementary to this, the FEL pulse energy is also reconstructed from the observed energy loss of the electron beam. This is achieved by recording the energy difference between lasing-on and lasing-off conditions using a beam-position monitor placed at a location exhibiting dispersion 30 m downstream of the undulator. The FEL pulse energy is calculated as the product of the electron energy loss and the number of electrons in the bunch as determined by the total bunch charge. Finally, the FEL transverse distribution is measured on a transverse profile monitor situated 32 m downstream of the undulator exit.

In the following, we report on the performance achieved for radiation wavelengths of 0.75 Å (≈16.5 keV photon energy) and 0.83 Å (≈15 keV). The data presented include measurements of the electron and photon beams obtained during a single experimental shift encompassing photon spectral measurements, pulse energies, and gain curves (with equivalent performance consistently reproduced during another measurement shift). The electron beam energy was 6.18 GeV at the standard bunch charge of 200 pC. The undulator K value was set at 1.104 for 0.83 Å and 0.956 for 0.75 Å. Below $K = 0.956$, although a small transverse spot characteristic of FEL radiation was still observable on transverse profile monitors downstream of the undulator screens, the pulse energy dropped below the measurable threshold of the gas monitor (i.e., below 10 μJ). Starting from an optimized machine that delivered 1 mJ pulse energy at 1 Å wavelength [20], we gradually decreased the wavelength to 0.75 Å. Several parameters were systematically tuned to maximize the pulse energy for both the 0.75 Å and 0.83 Å cases, including bunch compression, electron optics, beam tilt, undulator trajectory, K values of the individual undulator modules, undulator taper, and phase shifters.

Pulse energies measured by the gas monitor were in the range of 100–120 μJ at 0.75 Å and 360–380 μJ at 0.83 Å. The independent measurement based on the energy loss of the electron beam yielded 128 ± 14 μJ and 418 ± 43 μJ for the respective wavelengths of 0.75 Å and 0.83 Å (derived from five different measurements). Throughout this Letter, reported uncertainties and error bars represent the standard deviation of the measurements, unless otherwise specified. Regarding systematic uncertainties, the uncertainty of the gas monitor is estimated to be below 10%, dominated by the measurement of the gas pressure [29], while the systematic uncertainties of the energy loss approach (related to dispersion, electron beam energy, and charge) are estimated to be at the 1% level. Although the energy loss method yields slightly higher values, the two independent methods yield consistent results within their respective uncertainties.

Spectral measurements obtained by scanning the monochromator are shown in Fig. 2. The scans consisted of about 20 points with step sizes of 2.8×10^{-4} Å and 2.3×10^{-4} Å for radiation wavelengths of 0.83 and 0.75 Å, respectively. At each setting, we collected 500 shots, with each scan

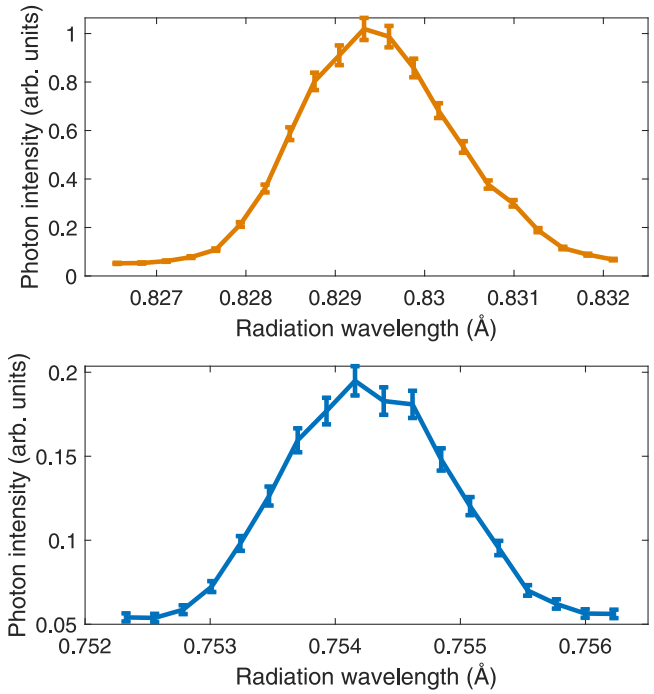


FIG. 2. Spectral measurements for radiation wavelengths of 0.83 Å (top) and 0.75 Å (bottom).

taking approximately 3 min. The expected central wavelengths calculated from the electron beam energy (6.18 GeV) and K values (1.104 and 0.956) are, according to the resonance condition, 0.825 and 0.747 Å. These values are slightly lower (by less than 1%) than the measured values (0.829 and 0.754 Å). The K values matching the measured wavelengths are 1.111 and 0.970, with a ±0.003 systematic uncertainty dominated by the 0.1% beam energy uncertainty. The systematic uncertainties of the nominal set values are dominated by the error in extrapolating the existing calibration performed for K values down to 1.2. They are estimated to be 0.011 for $K = 1.104$ and 0.048 for $K = 0.956$. The two methods of determining the K values agree well, considering the respective uncertainties. The spectral bandwidths are approximately 0.2% (full width at half maximum, FWHM). This value reflects the measured width of the averaged spectrum without deconvolution, including contributions from photon energy and bandwidth jitters.

Figure 3 displays the current profile and the time-resolved or slice emittance of the electron beam measured before energy collimator. For the emittance measurement, we subtract an emittance resolution of 34 nm to account for a profile resolution of 14 μm [24]. This emittance resolution is calculated according to [30] as the square of the profile monitor resolution multiplied by the electron beam Lorentz factor ($\gamma = 12\,094$) and divided by the β function at the screen during the measurement (70 m). The estimated resolution corresponds to a maximum of 15% of the measured emittances. As evident in the figure, the current

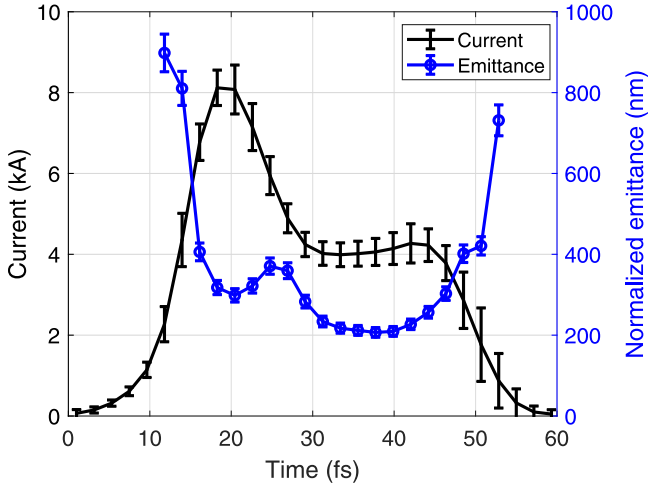


FIG. 3. Current profile and slice emittance measurement of the electron beam.

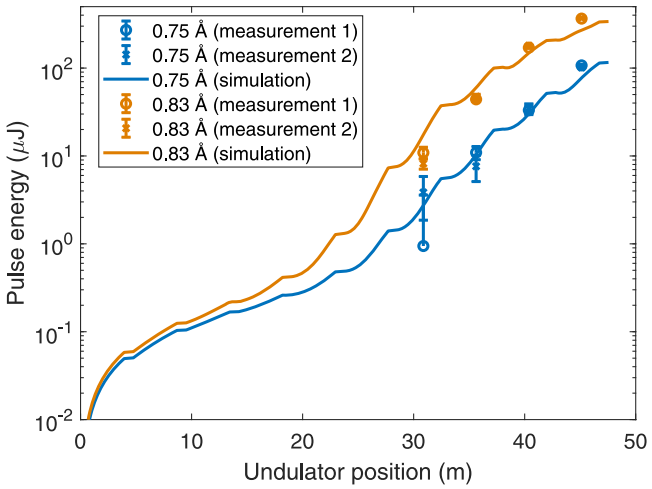


FIG. 4. Measured and simulated FEL gain curves for radiation wavelengths of 0.75 Å and 0.83 Å.

profile exhibits two distinct regions: the head of the bunch (left part of the plot) with a peak current up to 8 kA, and the core and tail sections (center and right parts) with a relatively constant peak current of approximately 4–4.5 kA. In standard operation, the electron beam is typically compressed to approximately 3 kA; however, higher compression was required for optimal performance in the subangstrom regime. Slice emittance values are 300–400 nm at the head of the bunch and 200–300 nm at the core and the tail. The slice energy spread was not directly measured during these commissioning shifts. Nevertheless, based on recent experience (see, e.g., Ref. [31]), it is estimated that it is approximately 1.2 MeV for 3 kA peak current, which scales to 1.6 MeV for 4 kA and 3.2 MeV for 8 kA under the assumption of constant longitudinal emittance.

A key improvement over early SwissFEL operation [11,30] is the enhanced ability to compress the electron bunch significantly further without compromising slice emittance or energy spread. The slice emittance values at the core and tail of the electron beam are comparable to those measured during the early stages of the project, but with significantly higher peak currents (4 kA) than before (1.5–2 kA). This is attributed to various improvements and optimizations [20], particularly a lower initial electron energy spread, achieved by reducing the longitudinal dispersion of the laser heater chicane in the injector [32] and the fine-tuning of many parameters (such as beam optics) to minimize collective effects.

The measured and simulated gain curves for 0.75 Å and 0.83 Å are shown in Fig. 4. Two independent measurement sets were collected for each wavelength. The gas monitor provided reliable measurements for pulse energies of at least several microjoules. The simulations were performed with GENESIS 1.3 [33] using the electron beam parameters measured or estimated earlier (see, e.g., Fig. 3), assuming the K values derived from the spectral measurements. To replicate experimental conditions, we considered 10 undulator modules in the simulations instead of 13, since it was experimentally verified during the shift that the first 3 undulator modules did not contribute to the gain, most likely due to residual trajectory errors. Moreover, the measurements were shifted by half a module, since the fourth undulator module was found to contribute only partially to the FEL process, yielding an effective active undulator length of 9.5 modules (38 m) for the experiment. The postsaturation taper [34] in the simulations was optimized to maximize pulse energy similarly to the machine configuration. The gain lengths calculated from the first three measurement points (out of four) are 3.0 m for a radiation wavelength of 0.75 Å and 2.7 m for 0.83 Å. These values are in good agreement with the simulated gain lengths calculated over the same undulator sections (including one additional module upstream), which yield 3.2 m and 2.7 m for 0.75 Å and 0.83 Å, respectively.

The good agreement between the measured and simulated gain curves validates our characterization of the electron beam and confirms the overall consistency of our experimental and numerical results. In both cases, the FEL process has reached or approached saturation. This is indicated by the reduction of the gain toward the end of the undulator line, marking the transition from exponential growth to saturation. The simulated FEL pulse duration is approximately 25 fs (FWHM), roughly corresponding to the bunch region (see Fig. 3) with peak current ≥ 4 kA and emittance ≤ 400 nm. However, the simulations show that for the measured beam distribution and the assumed energy spread scaling, the lower emittance part of the bunch appears to dominate the FEL output despite its lower peak current. Calculations based on the Ming Xie model [5], accounting for emittance and energy spread deterioration with peak current, confirm that, for our bunch charge of

200 pC, a peak current of approximately 4 kA with 200 nm emittance corresponds to optimum performance. The simulated maximum peak power of the FEL pulses is approximately 30 GW for 0.75 Å and 60 GW for 0.83 Å, which is remarkably high considering the low K values employed in this configuration.

We have simulated the FEL performance at 0.75 Å, varying the slice energy spread by ±25% relative to the baseline value. The gain curve and pulse energies show a strong dependence on the slice energy spread. Notably, the pulse energies change by an approximate factor of 2, scaling inversely with the variations in energy spread. This highlights the sensitivity of our operating point to the energy spread, and hence, the importance of minimizing the energy spread, and it confirms that our baseline energy spread is accurate.

The transverse distribution of the FEL radiation was characterized by measuring 50 consecutive shots on a profile monitor located 32 m downstream of the undulator. For a radiation wavelength of 0.75 Å, the average root mean square transverse size across all 50 shots was 62.5 ± 1.6 μm in the horizontal plane and 59.1 ± 1.0 μm in the vertical. The measured shot-to-shot stability shows a 7% intensity jitter (consistent with the gas monitor data) and a trajectory jitter of 12% and 4% of the spot size in the horizontal and vertical planes, respectively. Comparable stability was also recorded at the 0.83 Å wavelength. These stability metrics are consistent with standard operation, where the worse horizontal trajectory stability arises from the coupling of electron bunch compression to the horizontal plane.

In conclusion, we have demonstrated the generation of subangstrom FEL radiation at SwissFEL using a 6.2 GeV electron beam, an undulator period of 15 mm, and a K parameter of unity and below. This was made possible by the generation of extremely brilliant electron beams (more than 4 kA with 200 nm emittance or 8 kA with 300 nm), which represent new benchmarks for electron linear accelerators. This operational regime has already been validated through successful user experiments and will be made available in future calls for proposals to broaden the SwissFEL scientific capabilities. We plan to further enhance this regime to achieve higher pulse energies and shorter wavelengths by optimizing the electron beam quality. In the midterm, this may include the utilization of higher-charge electron beams with higher peak currents, as this could further improve the performance according to the Ming Xie model [5]; however, this would also introduce stronger collective effects that could deteriorate the performance. In the longer term, we plan to upgrade the rf photoinjector to improve the overall six-dimensional beam brilliance [35]. Additionally, we will implement K-value calibrations specifically for the subunity regime and refine alignment procedures to enhance operational efficiency at these shorter wavelengths.

Our results confirm that high-brilliance electron beams can successfully produce high-power radiation despite the reduced coupling associated with low values. Consequently, this Letter suggests a promising path toward more compact and cost-effective facilities by prioritizing electron beam quality, although a complete facility design with rigorous modeling of saturation lengths and tolerance studies would be required. For instance, using the 15 mm period and $K = 0.97$ reported here, 1 Å radiation could, in principle, be produced with a 5.37 GeV beam—a significant reduction compared to the original SwissFEL design energy of 5.8 GeV. Similarly, 1 nm soft x-ray pulses could potentially be achieved at 1.69 GeV, a considerably lower energy than in other facilities, such as the 2.5 GeV planned for the future S^{3}FEL in China [36]. Additional enhancements in electron beam quality, combined with short undulator periods and low K values, offer a compelling strategy to further reduce energy requirements, thus enabling a new generation of compact, high-performance x-ray sources.

Acknowledgments—We thank John Beale and the Cristallina team at SwissFEL for stimulating our work by requesting subangstrom FEL radiation for their crystallography experiments. We acknowledge the support of all technical groups involved in the operation of SwissFEL.

Data availability—The data that support the findings of this article are not publicly available. The data are available from the authors upon reasonable request.

[1] C. Pellegrini, A. Marinelli, and S. Reiche, The physics of x-ray free-electron lasers, Rev. Mod. Phys. **88**, 015006 (2016).

[2] E. A. Seddon, J. A. Clarke, D. J. Dunning, C. Masciovecchio, C. J. Milne, F. Parmigiani, D. Rugg, J. C. H. Spence, N. R. Thompson, K. Ueda, S. M. Vinko, J. S. Wark, and W. Wurth, Short-wavelength free-electron laser sources and science: A review, Rep. Prog. Phys. **80**, 115901 (2017).

[3] R. Bonifacio, C. Pellegrini, and L. M. Narducci, Collective instabilities and high-gain regime in a free electron laser, Opt. Commun. **50**, 373 (1984).

[4] E. Saldin, E. Schneidmiller, and M. Yurkov, Coherence properties of the radiation from x-ray free electron laser, Opt. Commun. **281**, 1179 (2008).

[5] M. Xie, Exact and variational solutions of 3d eigenmodes in high gain FELs, Nucl. Instrum. Methods Phys. Res., Sect. A **445**, 59 (2000).

[6] P. Emma *et al.*, First lasing and operation of an ångstrom-wavelength free-electron laser, Nat. Photonics **4**, 641 (2010).

[7] Y. Ding, LCLS-II commissioning and operation with high-repetition-rate CW FELs, in *Proceedings of the 16th International Particle Accelerator Conference, Taipei, Taiwan* (JACoW, Geneva, Switzerland, 2025), pp. 1710–1713.

[8] T. Ishikawa *et al.*, A compact x-ray free-electron laser emitting in the sub-ångström region, Nat. Photonics **6**, 540 (2012).
[9] H.-S. Kang *et al.*, Hard x-ray free-electron laser with femtosecond-scale timing jitter, Nat. Photonics **11**, 708 (2017).
[10] W. Decking *et al.*, A MHz-repetition-rate hard x-ray free-electron laser driven by a superconducting linear accelerator, Nat. Photonics **14**, 391 (2020).
[11] E. Prat *et al.*, A compact and cost-effective hard x-ray free-electron laser driven by a high-brightness and low-energy electron beam, Nat. Photonics **14**, 748 (2020).
[12] Z. Zhao, D. Wang, Z.-H. Yang, and L. Yin, SCLF: An 8-GeV CW SCRF linac-based X-ray FEL facility in Shanghai, in *Proceedings of the 38th International Free Electron Laser Conference, Santa Fe, New Mexico, USA* (JACoW, Geneva, Switzerland, 2018).
[13] K. Takaba, S. Maki-Yonekura, I. Inoue, K. Tono, T. Hamaguchi, K. Kawakami, H. Naitow, T. Ishikawa, M. Yabashi, and K. Yonekura, Structural resolution of a small organic molecule by serial x-ray free-electron laser and electron crystallography, Nat. Chem. **15**, 491 (2023).
[14] K. H. Kim *et al.*, Direct observation of bond formation in solution with femtosecond x-ray scattering, Nature (London) **518**, 385 (2015).
[15] A. I. Chumakov, A. Q. R. Baron, I. Sergueev, C. Strohm, O. Leupold, Y. Shvyd'ko, G. V. Smirnov, R. Rüffer, Y. Inubushi, M. Yabashi, K. Tono, T. Kudo, and T. Ishikawa, Superradiance of an ensemble of nuclei excited by a free electron laser, Nat. Phys. **14**, 261 (2017).
[16] M. Gerharz *et al.*, Single-shot sorting of Mössbauer time-domain data at x-ray free electron lasers, arXiv:2509.15833.
[17] J. Griffiths, A. F. Suzana, L. Wu, S. D. Marks, V. Esposito, S. Boutet, P. G. Evans, J. F. Mitchell, M. P. M. Dean, D. A. Keen, I. Robinson, S. J. L. Billinge, and E. S. Bozin, Resolving length-scale-dependent transient disorder through an ultrafast phase transition, Nat. Mater. **23**, 1041 (2024).
[18] A. F. Sapnik *et al.*, High-quality ultra-fast total scattering and pair distribution function data using an x-ray free-electron laser, IUCrJ **12**, 531 (2025).
[19] H. P. Liermann *et al.*, Novel experimental setup for megahertz x-ray diffraction in a diamond anvil cell at the High Energy Density (HED) instrument of the European X-ray Free-Electron Laser (EuXFEL), J. Synchrotron Radiat. **28**, 688 (2021).
[20] C. Kittel, M. Aiba, C. Arrell, A. Cassar, E. Ferrari, N. Hiller, E. Prat, S. Reiche, N. Sammut, T. Schietinger, D. Voulot, T. Weilbach, and M. Calvi, Enhancing hard x-ray beamline performance at SwissFEL through spontaneous radiation measurements, J. Synchrotron Radiat. **33**, 32 (2026).
[21] E. Prat, P. Dijkstal, E. Ferrari, and S. Reiche, Demonstration of large bandwidth hard x-ray free-electron laser pulses at SwissFEL, Phys. Rev. Lett. **124**, 074801 (2020).
[22] E. Prat, A. Malyzhenkov, and P. Craievich, Sub-femtosecond time-resolved measurements of electron bunches with a C-band radio-frequency deflector in x-ray free-electron lasers, Rev. Sci. Instrum. **94**, 043103 (2023).
[23] R. Ischebeck, E. Prat, V. Thominet, and C. Ozkan Loch, Transverse profile imager for ultrabright electron beams, Phys. Rev. ST Accel. Beams **18**, 082802 (2015).
[24] P. Juranić and E. Prat, Testing high-resolution transverse profile monitors by measuring the dependence of the electron beam size on the beam energy at SwissFEL, Rev. Sci. Instrum. **94**, 073301 (2023).
[25] C. David, G. Seniutinas, M. Makita, B. Rösner, J. Rehanek, P. Karvinen, F. Löhl, R. Abela, L. Patthey, and P. Juranić, Spectral monitoring at SwissFEL using a high-resolution on-line hard X-ray single-shot spectrometer, J. Synchrotron Radiat. **28**, 1978 (2021).
[26] R. Follath, U. Flechsig, C. J. Milne, J. Szlachetko, G. Ingold, B. Patterson, L. Patthey, and R. Abela, Optical design of the ARAMIS-beamlines at SwissFEL, AIP Conf. Proc. **1741**, 020009 (2016).
[27] G. Ingold *et al.*, Experimental station Bernina at SwissFEL: Condensed matter physics on femtosecond time scales investigated by x-ray diffraction and spectroscopic methods, J. Synchrotron Radiat. **26**, 874 (2019).
[28] A. A. Sorokin, Y. Bican, S. Bonfigt, M. Brachmanski, M. Braune, U. F. Jastrow, A. Gottwald, H. Kaser, M. Richter, and K. Tiedtke, An x-ray gas monitor for free-electron lasers, J. Synchrotron Radiat. **26**, 1092 (2019).
[29] P. Juranić *et al.*, SwissFEL Aramis beamline photon diagnostics, J. Synchrotron Radiat. **25**, 1238 (2018).
[30] E. Prat, P. Dijkstal, M. Aiba, S. Bettoni, P. Craievich, E. Ferrari, R. Ischebeck, F. Löhl, A. Malyzhenkov, G. L. Orlandi, S. Reiche, and T. Schietinger, Generation and characterization of intense ultralow-emittance electron beams for compact x-ray free-electron lasers, Phys. Rev. Lett. **123**, 234801 (2019).
[31] E. Prat, C. Kittel, M. Calvi, P. Craievich, P. Dijkstal, S. Reiche, T. Schietinger, and G. Wang, Experimental characterization of the optical klystron effect to measure the intrinsic energy spread of high-brightness electron beams, Phys. Rev. Accel. Beams **27**, 030701 (2024).
[32] E. Prat, P. Craievich, P. Dijkstal, S. Di Mitri, E. Ferrari, T. G. Lucas, A. Malyzhenkov, G. Perosa, S. Reiche, and T. Schietinger, Energy spread blowup by intrabeam scattering and microbunching at the SwissFEL injector, Phys. Rev. Accel. Beams **25**, 104401 (2022).
[33] S. Reiche, GENESIS 1.3: A fully 3D time-dependent FEL simulation code, Nucl. Instrum. Methods Phys. Res., Sect. A **429**, 243 (1999).
[34] N. Kroll, P. Morton, and M. Rosenbluth, Free-electron lasers with variable parameter wigglers, IEEE J. Quantum Electron. **17**, 1436 (1981).
[35] C. Bostedt *et al.*, SwissFEL+ conceptual design report, PSI Report No. 26-01 2026.
[36] X. Wang, L. Zeng, J. Shao, Y. Liang, H. Yi, Y. Yu, J. Sun, X. Li, C. Feng, Z. Wang, S. Zhao, H. Jia, S. Huang, W. Zhang, and X. Yang, Physical design for Shenzhen superconducting soft x-ray free-electron laser (S^3FEL), in *Proceedings of the 14th International Particle Accelerator Conference, Venice, Italy* (JACoW, Geneva, Switzerland, 2023), pp. 1852–1855.

Correction: A typographical error in the last sentence of the final paragraph preceding the Acknowledgments has been corrected.